





LGMD-Driven Collision Avoidance

Appendix

A. Model Comparison

The proposed Bio-inspired LGMD model is compared with the most similar model as listed in the following table.

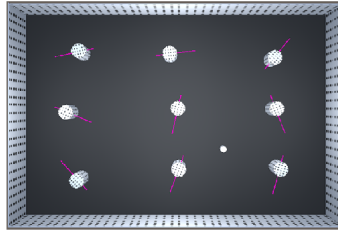
Appendix Table I
Performance Comparison between Previous Method and Our Proposed Model

Method	 Square cube (0.4m×0.4m×0.4m)	 Wide cube (0.4m×1m×0.4m)	 High cube (0.4m×0.4m×1m)	 Long cube (1m×0.4m×0.4m)	Average
Yue <i>et al.</i> [Appendix 1]	100%	77.78% (28/36)	100%	100%	92.59% (100/108)
Ours	95.83% (23/24)	97.22% (35/36)	91.67% (22/24)	95.83% (23/24)	95.37% (103/108)

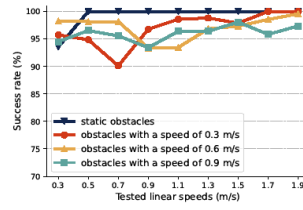
[Appendix 1] S. Yue, R. D. Santer, Y. Yamawaki, and F. C. Rind, “Reactive direction control for a mobile robot: a locust-like control of escape direction emerges when a bilateral pair of model locust visual neurons are integrated,” *Autonomous Robots*, vol. 28, no. 2, pp. 151–167, 2010.

B. Performance Test

Static and dynamic obstacles are used to test our proposed method. Dynamic obstacles can move back and forth in a random direction at different speeds (as Appendix Fig. 1). Appendix Fig. 2 illustrates that the success rates of a mobile robot at different speeds for collision detection and avoidance against static obstacles and dynamic obstacles are all above 90% with satisfactory performance. Except for the slow speed of 0.3 m/s, the success rates of a mobile robot against static obstacles are all 100%. This paves a solid basis for real-world autonomy by simulating the driving situations from our ego-vehicle and other dynamic motion cues.



Appendix Fig. 1. The dynamic obstacles move back and forth in the arena, and purple lines represent the moving trajectories of the obstacles.

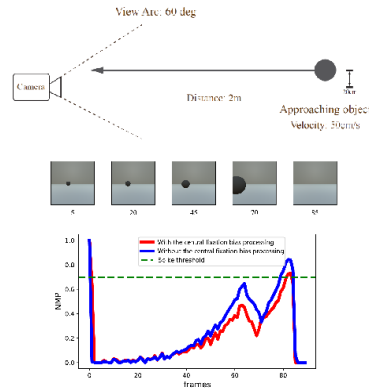


Appendix Fig. 2. The success rate of a mobile robot at nine individual linear speeds for collision detection and avoidance in static and dynamic obstacles test.

C. Human Factor in Driving: Impact of central fixation bias

The processing of central fixation bias plays a selective role in near-approaching stimuli. When stimuli approached from the side, due to the processing of central fixation bias, the weight of the image edge was lower, which suppressed the growth of normalized membrane potentials (NMPs), thereby reducing false collision detections caused by the stimuli passing from the side. Therefore, the proposed LGMD model demonstrates better sensitivity to frontal approaching objects.

We have conducted experiments to show the impact of central fixation bias. We set a sphere to approach the camera at 50 cm/s at different vertical distances as shown in the subfigure above. The subfigure below demonstrates that our proposed central fixation bias processing plays a selective role in near-approaching stimuli. When stimuli approached from the side, due to the central fixation bias processing, the weight of the image edge was lower, which suppressed the growth of NMP, thereby reducing false collision detections caused by the stimuli passing from the side. Benefitting from this central fixation bias mechanism, the proposed LGMD model demonstrates better sensitivity to frontal approaching objects.



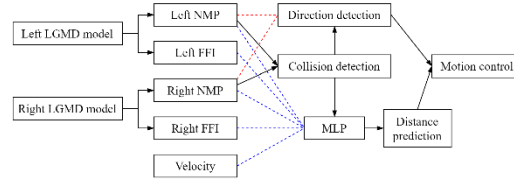
Appendix Fig. 3. Comparison results of the proposed model with the model without center-biased processing.

D. Human Factor in Driving: Binocular Vision

Binocular vision plays a key role in optimal direction selection and distance prediction which provides an obvious improvement over traditional monocular LGMD.

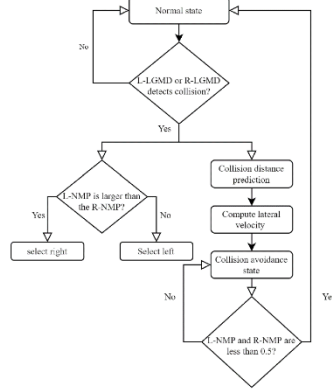
In detail, these two functions are combined for our binocular robot, and their functions are discussed below.

1. Direction Selection: As shown in the following figure, we determine the collision avoidance direction by comparing the NMPs from the left and right LGMD models. The LGMD model with a larger NMP will be the "winner", and the robot will choose the opposite direction as the optimal collision direction. This algorithm is triggered when either the left or right LGMD model detects a collision.



Appendix Fig. 4. Diagram of binocular LGMD-based direction selection strategy for collision avoidance.

2. Distance Prediction: A multilayer perceptron (MLP) is utilized to train the output features of two LGMD models to predict distance. The following figure shows the schematic diagram of the motion control flow chart of our proposed binocular vision system.



Appendix Fig. 5. The motion control flow chart of our proposed binocular system.

E. Advantages of Bio-inspired Approach

Rather than using deep learning or other high-cost GPU and CPU devices, the bio-inspired approach has its unique dominance for next-generation automation, which provides its computational simplicity, flexibility, and robustness for autonomous micro-mobile robots.

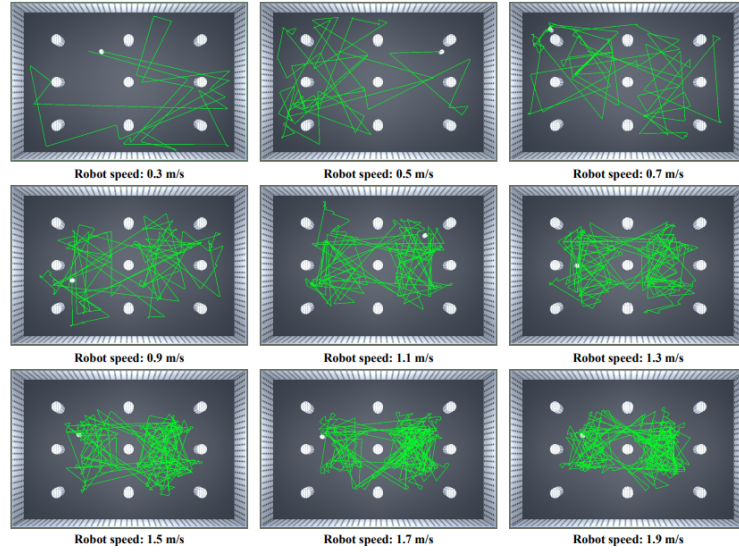
[Appendix 2] Y. J. Heo, D. Kim, W. Lee, H. Kim, J. Park, and W. K. Chung, "Collision Detection

for Industrial Collaborative Robots: A Deep Learning Approach,” *IEEE Robotics and Automation Letters*, vol. 4, no. 2, pp. 740–746, April 2019, doi: 10.1109/LRA.2019.2893400.

[Appendix 3] H. Chae, C. M. Kang, B. Kim, J. Kim, C. C. Chung, and J. W. Choi, “Autonomous braking system via deep reinforcement learning,” *IEEE 20th International Conference on Intelligent Transportation Systems (ITSC)*, 2017, pp. 1–6, doi: 10.1109/ITSC.2017.8317839.

F. Mobile Robot Tests

To test the effectiveness and robustness of the proposed LGMD model on the mobile robot, we put a mobile robot in the arena with multiple obstacles to examine whether mobile robots can detect obstacles precisely and then avoid them timely. The size of the arena is $15\text{m} \times 10\text{m}$, and the duration of each test is set to 7 minutes. In the tests of the arena as Appendix Fig. 6, a mobile robot moves forward autonomously until a potential collision threat is detected. To avoid collisions, the mobile robot will stop moving forward, turn right or left randomly with a large angle ranging from 90 degrees and 150 degrees, and then continue moving forward. Besides, for each subfigure in Appendix Fig. 6, the trajectories of the robot in the arena are recorded from the lowest speed to the highest speed (from 0.3m/s – 4m/s).



Appendix Fig. 6. The captures of our mobile test for collision avoidance in field tests.